Error estimation for the polygonal finite element method for smooth and singular linear elasticity

Octavio Andrés González Estrada, Sundararajan Natarajan, Juan José Ródenas, Stéphane P.A. Bordas

▶ **To cite this version:**

Octavio Andrés González Estrada, Sundararajan Natarajan, Juan José Ródenas, Stéphane P.A. Bordas. Error estimation for the polygonal finite element method for smooth and singular linear elasticity. Computers & Mathematics with Applications, 2021, 92, pp.109-119. 10.1016/j.camwa.2021.03.017 . hal-03201137

HAL Id: hal-03201137
https://hal.science/hal-03201137v1

Submitted on 8 Oct 2021

HAL is a multi-disciplinary open access archive for the deposit and dissemination of scientific research documents, whether they are published or not. The documents may come from teaching and research institutions in France or abroad, or from public or private research centers.

L'archive ouverte pluridisciplinaire **HAL**, est destinée au dépôt et à la diffusion de documents scientifiques de niveau recherche, publiés ou non, émanant des établissements d'enseignement et de recherche français ou étrangers, des laboratoires publics ou privés.

Error estimation for the polygonal finite element method for smooth and singular linear elasticity

Octavio A. González-Estrada[1] Sundararajan Natarajan[2]
Juan José Ródenas[3] Stéphane P.A. Bordas[1,4,*]

March 10, 2021

[1]School of Mechanical Engineering, Universidad Industrial de Santander, Ciudad Universitaria, Bucaramanga, Colombia, e-mail: agonzale@uis.edu.co (orcid:0000-0002-2778-3389)
[2]Department of Mechanical Engineering, Indian Institute of Technology Madras, Chennai 600036, India, e-mail: snatarajan@iitm.ac.in (orcid:0000-0002-0409-0096)
[3]Centro de Investigación en Ingeniería Mecánica (CIIM), Universitat Politècnica de València, Camino de Vera s/n, E-46022-Valencia, Spain, e-mail: jjrodena@mcm.upv.es (orcid:00000-0003-2195-7920)
[4]Universitè du Luxembourg, Research unit of Engineering Science, Campus Kirchberg, 6 rue Richard Coudenhove-Kalergi, L-1359 Luxembourg, e-mail: stephane.bordas@alum.northwestern.edu (orcid:0000-0001-7622-2193)

Abstract

A recovery-based error indicator developed to evaluate the quality of polygonal finite element approximations is presented in this paper. Generalizations of the finite element method to arbitrary polygonal meshes have been increasingly investigated in the last years, as they provide flexibility in meshing and improve solution accuracy. As any numerical approximation, they have an induced error which has to be accounted for in order to validate the approximate solution. Here, we propose a recovery type error measure based on a moving least squares fitting of the finite element stress field. The quality of the recovered field is improved by imposing equilibrium conditions and, for singular problems, splitting the stress field into smooth and singular parts. We assess the performance of the error indicator using three problems with exact solution, and we also compared the results with those obtained with standard finite element meshes based on simplexes. The results indicate good values for the local and global effectivities, similar to the values obtained for standard approximations, and are always within the recommended range.

Keywords: polygonal finite element method; Laplace interpolants; error estimation; statical admissibility; singularity; recovery

1 Introduction

Mathematically, a real physical process can be recast in terms of governing partial differential equations (PDEs). One of the most robust numerical methods to the solution of PDEs is the finite element method (FEM). In general, numerical methods provide an approximated solution to the physical problem under consideration. The approximated solution exhibits an error which has to be quantified to validate the numerical model. Error estimation and error control techniques have been intensively researched for the FEM and robust procedures are already available [1]. In particular, we are interested in the family of recovery-based error estimation techniques first introduced by [2]. Recovery methods based on stress smoothing are often preferred for practical applications among the engineering community, mostly because very simple procedures can yield good results. Simple nodal averaging, superconvergent patch recovery (SPR) [3] or moving least squares approaches [4–6] are common in the literature [7]. Stress smoothing yields good values of effectivity globally for a given mesh, but is known to have problems locally, especially along the boundaries, where stress values are normally of interest. This condition poses a problem for the error indicator to guide adaptivity algorithms. To overcome this difficulty, a balance between the stress smoothing techniques and approaches based on equilibrium have been proposed [6,8]. The aforementioned error estimation techniques have been successfully applied to advanced discretization techniques such as the XFEM, the smoothed finite element method (SFEM) to name a few in [6,9,10]. The earlier studies were restricted to quadrilateral and triangular elements in two dimensions and, tetrahedral and hexahedral elements in three dimensions. Recently, finite elements in the shape of pentagons, hexagons and in general $n-$sided polygons (and polyhedral elements in three dimensions) have attracted attention in the research community, both in computational physics [11–16] and in computer graphics [17, 18]. In the early 1970s, Wachspress derived a systematic approach to construct basis functions over arbitrary polygonal domains in his famous book on the rational finite element method [19]. *Polygonal finite elements*, which are not limited to have up to four sides in two dimensions or up to six faces in three dimensions, started with the seminal works from [12, 20, 21]. A non-conforming method, called the variable element topology finite element method (VETFEM), was proposed in [22], and uses a constrained minimization procedure to construct shape functions for convex and non-convex elements, computed in the physical space ($\mathbf{x} \in \Omega$). The Voronoï cell finite element model (VCFEM) was introduced in [11, 23, 24] for modeling heterogeneous microstructures of composites and porous materials with heterogeneities of regular shapes, incorporating a hybrid assumed stress formulation. The cells in the VCFEM do not conform to the strict definitions of Voronoï cells as they are, in general, arbitrary. In [25], a conformal mapping method was developed to investigate microstructures with irregular heterogeneities. Other recent formulations include the polygonal elements based on the virtual nodes [26], the virtual element methods (VEM) [27] and the scaled boundary polygon finite element method [28, 29], strain smoothing technique [30], BEM-based FEM [31] and $hp-$clouds [32]. In [33], a connection between the hourglass control and the VEM was showed, and in [34], a connection between the cell based smoothed finite element

method and the VEM.
The study of the error in novel types of numerical approximations, e.g. arbitrary polygonal FEM, has to be considered in order to be able to guarantee the numerical results in practical applications. In the case of polygonal elements, first attempts using residual-based error measures can be found in [35, 36]. More recently, *a priori* error analysis for polygonal meshes has been performed in [37] and *a posteriori* residual based error estimates have been investigated in [38] for the virtual element method. Regarding recovery-based error estimates using gradient smoothing, first approaches have been presented in [39, 40], and more recently in [41].

In this paper, we present the use of a recovery-based error indicator for arbitrary polygonal finite element approximations, which uses an enhanced moving least squares approach to smooth the raw stress field. The paper is organised as follows: In section 2, we introduce the linear elasticity problem under consideration and its approximated solution using polygonal FEM. In section 3 we explain the methodology for recovery based error estimation, and the proposed approach for polygonal elements. Then, in section 4 we validate the error estimation procedure using benchmark problems with exact solution, both for smooth and singular problems. Finally, we present some concluding remarks.

2 Linear elasticity problem and finite element approximation

In this section, we introduce the linear elasticity problem under consideration for two dimensions. Using Voigt notation, we denote the Cauchy stress by $\boldsymbol{\sigma} = \{\sigma_{xx}, \sigma_{yy}, \sigma_{xy}\}^T$, the displacement by $\mathbf{u} = \{u_x, u_y\}^T$ and the strain by $\boldsymbol{\varepsilon} = \{\varepsilon_{xx}, \varepsilon_{yy}, \varepsilon_{xy}\}^T$. These fields are defined over a domain $\Omega \subset \mathbb{R}^2$, bounded by the boundary $\partial\Omega$. The boundary accommodates the following decompositions: Neumann and Dirichlet boundary as $\partial\Omega = \Gamma_N \cup \Gamma_D$ and $\Gamma_N \cap \Gamma_D = \emptyset$. Prescribed tractions, denoted by $\mathbf{t}$, are imposed over the Neumann boundary, Γ_N, while displacements, denoted by $\bar{\mathbf{u}}$, are prescribed over the complementary part of the boundary, Γ_D. The body load is denoted by $\mathbf{b}$. The elasticity problem takes the following form. We seek $(\boldsymbol{\sigma}, \mathbf{u})$ satisfying:

$$\mathbf{L}^T\boldsymbol{\sigma} + \mathbf{b} = \mathbf{0} \qquad \text{in } \Omega, \tag{1}$$

$$\mathbf{G}\boldsymbol{\sigma} = \mathbf{t} \qquad \text{on } \Gamma_N, \tag{2}$$

$$\mathbf{u} = \bar{\mathbf{u}} \qquad \text{on } \Gamma_D, \tag{3}$$

$$\boldsymbol{\varepsilon}(\mathbf{u}) = \mathbf{L}\mathbf{u} \qquad \text{in } \Omega, \tag{4}$$

$$\boldsymbol{\sigma} = \mathbf{D}\Big[\boldsymbol{\varepsilon}(\mathbf{u}) - \boldsymbol{\varepsilon}_0\Big] + \boldsymbol{\sigma}_0 \qquad \text{in } \Omega, \tag{5}$$

in the above expressions, $\mathbf{D}$ represents the standard elasticity matrix of the constitutive relation between the stress and the strain for linear isotropic materials, $\boldsymbol{\sigma}_0$ represents the initial stress and $\boldsymbol{\varepsilon}_0$ the initial strain. $\mathbf{L}$ is the linear differential operator and $\mathbf{G}$ is the operator that projects the stresses onto tractions over the

Neumann boundary considering the unit normal $\mathbf{n}$ to Γ_N:

$$\mathbf{L}^T = \begin{bmatrix} \partial/\partial x & 0 & \partial/\partial y \\ 0 & \partial/\partial y & \partial/\partial x \end{bmatrix}, \qquad \mathbf{G} = \begin{bmatrix} n_x & 0 & n_y \\ 0 & n_y & n_x \end{bmatrix}$$

The variational form of the linear elasticity problem can be written as:

$$\begin{aligned} &\text{Find } \mathbf{u} \in V \text{ such that } \forall \mathbf{v} \in V : \\ &\int_\Omega \boldsymbol{\varepsilon}(\mathbf{v})^{\mathrm{T}} \mathbf{D} \boldsymbol{\varepsilon}(\mathbf{u}) \mathrm{d}\Omega = \\ &\int_\Omega \mathbf{v}^{\mathrm{T}} \mathbf{b} \mathrm{d}\Omega + \int_{\Gamma_{\mathrm{N}}} \mathbf{v}^{\mathrm{T}} \mathbf{t} \mathrm{d}\Gamma + \int_\Omega \boldsymbol{\varepsilon}(\mathbf{v})^{\mathrm{T}} \mathbf{D} \boldsymbol{\varepsilon}_0 \mathrm{d}\Omega - \int_\Omega \boldsymbol{\varepsilon}(\mathbf{v})^{\mathrm{T}} \boldsymbol{\sigma}_0 \mathrm{d}\Omega \end{aligned} \tag{6}$$

with $V = \{\mathbf{v} \mid \mathbf{v} \in [H^1(\Omega)]^2, \mathbf{v}|_{\Gamma_D} = \mathbf{0}\}$. The approximate displacement solution $\mathbf{u}^h$ is found in a finite dimensional space $V^h \subset V$, spanned by the finite element basis functions with local support. Using the Galerkin approach, the variational form (6) takes the form:

$$\begin{aligned} &\text{Find } \mathbf{u}^h \in V^h \text{ such that } \forall \mathbf{v} \in V^h : \\ &\int_\Omega \boldsymbol{\varepsilon}(\mathbf{v})^{\mathrm{T}} \mathbf{D} \boldsymbol{\varepsilon}(\mathbf{u}^h) \mathrm{d}\Omega = \\ &\int_\Omega \mathbf{v}^{\mathrm{T}} \mathbf{b} \mathrm{d}\Omega + \int_{\Gamma_{\mathrm{N}}} \mathbf{v}^{\mathrm{T}} \mathbf{t} \mathrm{d}\Gamma + \int_\Omega \boldsymbol{\varepsilon}(\mathbf{v})^{\mathrm{T}} \mathbf{D} \boldsymbol{\varepsilon}_0 \mathrm{d}\Omega - \int_\Omega \boldsymbol{\varepsilon}(\mathbf{v})^{\mathrm{T}} \boldsymbol{\sigma}_0 \mathrm{d}\Omega \end{aligned} \tag{7}$$

which can be solved using classical finite elements [7] or with the more recent polygonal finite element method (PFEM) [11, 20, 22–24, 42].

The PFEM can be seen as the generalization of the finite elements that allows the elements to take arbitrary shapes and size. The use of polygonal elements requires the computation of basis functions satisfying the following properties: partition of unity, interpolation, linear completeness and non-negativity. However, there is no unique way to represent these basis functions over arbitrary polytopes that satisfies the aforementioned properties. The basis functions over arbitrary polytopes are referred to as '*barycentric coordinates*' [19, 20, 43, 44].

Wachspress [19] investigated the construction of basis functions for any wedge form, also defining interpolants on arbitrary polygons. Sibson [45] proposed natural neighbor interpolants which are based on the Voronoï diagram. Voronoï interpolants have been broadly applied in mechanics [46–49]. During their studies on random lattices, Chris *et al.* [50] introduced a weighting functional based on the distance to the boundary. In the late 1990s, the Sibson [51] and Laplace [52] interpolants were re-discovered. For advances in polygonal elements, interested readers are referred to the literature [20, 53] and the references therein. In this study we consider only Wachspress shape functions with an isoparametric mapping. However, other shape functions can also be employed.

The Wachspress shape functions are rational functions and the construction of these coordinates is as follows: Let $P \subset \mathbb{R}^2$ be a simple convex polygon with vertices $v_i, i = 1, \cdots, n$, where n represents the number of sides of the convex polygon.

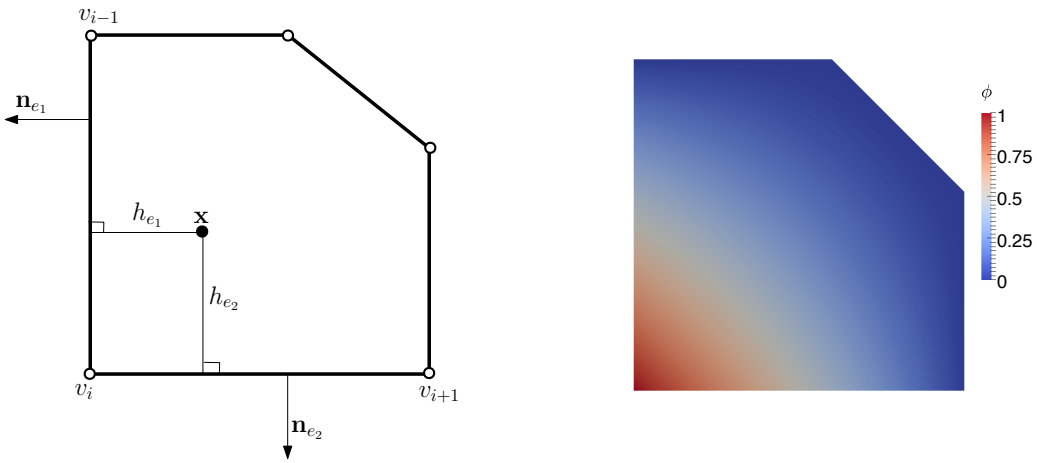

(a) (b)

Figure 1: Arbitrary pentagon: (a) definition of unit outward normals and perpendicular distances and (b) basis function for a vertex node.

For each edge $e \in \mathcal{E}(P)$, where $\mathcal{E}(P)$ represents the collection of edges of P, let $\mathbf{n}_e$ be the unit outward normal and for any $\mathbf{x} \in P$, let $h_e(\mathbf{x})$ denote the perpendicular distance of $\mathbf{x}$ to e, given by:

$$\mathbf{h}_e(\mathbf{x}) = (\mathbf{v} - \mathbf{x}) \cdot \mathbf{n}_e \tag{8}$$

for any vertex $\mathbf{v} \in \mathcal{V}(P)$ that belongs to e, where $\mathcal{V}(P)$ denotes the set of vertices of P. For each vertex $\mathbf{v} \in \mathcal{V}(P)$, let e_1, e_2 be the two edges incident to $\mathbf{v}$ and for $\mathbf{x} \in P$, let

$$w_{\mathbf{v}}(\mathbf{x}) = \frac{\det(\mathbf{n}_{e_1}, \mathbf{n}_{e_2})}{h_{e_1}(\mathbf{x}) h_{e_2}(\mathbf{x})} \tag{9}$$

with a condition that the ordering of e_1, e_2 be anticlockwise around the vertex $\mathbf{v}$ when seen from outside P (see Figure (1) for the definition of vertices, outward normal and perpendicular distances). Then, the Wachspress shape functions for $\mathbf{x} \in P$ is given by [19, 43]:

$$\phi_{\mathbf{v}}(\mathbf{x}) = \frac{w_{\mathbf{v}}(\mathbf{x})}{\sum\limits_{\mathbf{u} \in \mathcal{V}(P)} w_{\mathbf{u}}(\mathbf{x})} \tag{10}$$

Figure (1) shows a representative polygon and a shape function for a vertex node computed by the above expression.

The shape functions described above over arbitrary polygons are rational functions, hence the formulation of efficient integration rules and evaluation of their derivatives pose a particular challenge. This has received much attention in recent years [42, 54–56] as evidenced by the growing literature. One potential solution is to subdivide the physical element into triangles and, then, use available quadrature rules for the numerical integration over triangles [42]. Subdivision is introduced solely to facilitate the numerical integration and does not introduce additional unknowns. Although straightforward, this process involves a two-level isoparametric

mapping, and requires the positivity of the Jacobian matrix used for the transformation. Lyness and Monegato [57] presented quadrature rules for regions with hexagonal symmetry. Natarajan *et al.* [54] proposed a numerical integration technique over arbitrary polygons based on complex mapping. This procedure avoids the two-level isoparametric mapping while guaranteeing the positivity of the Jacobian, but is restricted to only two dimensions. Sommariva and Vianello [58] presented a Gauss-like cubature over arbitrary polygons. Mousavi *et al.* [55] presented a numerical algorithm based on group theory and an optimization scheme to compute integration rules over arbitrary polygons, and very recently Thiagarajan and Shapiro [59] presented an adaptively weighted numerical integration scheme over arbitrary domains. Based on Stokes' theorem and using the property of homogeneous functions, Chin *et al.,* [60] showed that integration over polytope can be reduced to integration over the boundary facets. Francis *et al.* [30] presented a modification to the constant smoothing scheme that recovers optimal convergence rates and yields better accuracy. For the present study, we employ sub-triangulation of the polygonal domain unless otherwise indicated.

3 Error estimates in the energy norm

3.1 Zienkiewicz–Zhu estimate

Let us assume that the difference between the exact solution and the finite element solution is only due to the finite size of the elements (i.e. geometrical modeling errors, numerical integration errors and other types of errors are considered negligible). Under this assumption, the discretisation error of the finite element approximation can be defined as $\mathbf{e} = \mathbf{u} - \mathbf{u}^h$. The error in energy norm $\|\mathbf{e}\|$ is normally used to quantify the quality of $\mathbf{u}^h$, and it is defined by:

$$\|\mathbf{e}\|^2 = \int_\Omega \mathbf{e}_\sigma^{\mathrm{T}} \mathbf{D}^{-1} \mathbf{e}_\sigma \mathrm{d}\Omega, \tag{11}$$

where the error in the stress field is denoted as $\mathbf{e}_\sigma = \boldsymbol{\sigma} - \boldsymbol{\sigma}^h$, and the finite element stress field is given by $\boldsymbol{\sigma}^h = \mathbf{D}\left(\boldsymbol{\varepsilon}(\mathbf{u}^h) - \boldsymbol{\varepsilon}_0\right) + \boldsymbol{\sigma}_0$.
A recovery-based estimate $\mathcal{E}$ of the exact error measure $\|\mathbf{e}\|$ can be approximated as [2]:

$$\|\mathbf{e}\|^2 \approx (\mathcal{E})^2 = \int_\Omega \left(\mathbf{e}_\sigma^*\right)^{\mathrm{T}} \mathbf{D}^{-1} \left(\mathbf{e}_\sigma^*\right) \mathrm{d}\Omega, \tag{12}$$

where $\mathbf{e}_\sigma^*$ denotes the approximate error in the stress field, defined by $\mathbf{e}_\sigma^* = \boldsymbol{\sigma}^* - \boldsymbol{\sigma}^h$, being $\boldsymbol{\sigma}^*$ the recovered stress field, evaluated as a postprocess of the FE solution. When $\boldsymbol{\sigma}^*$ converges to the exact stress field at a higher rate than the finite element solution, the estimate measure is considered asymptotically exact, meaning that the approximated error tends to the exact error as we refine the mesh [7]. Notice that the accuracy of the error estimate depends on the quality of the recovered stress field. Nodal averaging was used in [2] to obtain $\boldsymbol{\sigma}^*$, however, basic smoothing techniques provide good global effectivities but suffer from a local lack of accuracy. For example, simple recovery approaches, such as the standard superconvergent

patch recovery (SPR) [3], do not use the information from the boundary conditions, where the imposed tractions are known *a priori* and the patches can have less sampling points, thus, leading to a reported lack of accuracy of the recovered field along the Neumann boundary. To improve the quality of the recovered stress field, methods considering equilibrium conditions have been developed [6, 8, 61, 62]. In the next section, we describe a moving least squares (MLS) recovery scheme that considers equilibrium conditions and singular fields, applied to the problem of error estimation for arbitrary polygonal FE formulations.

3.2 Enhanced MLS recovery

The moving least squares recovery is a weighted least squares fitting defined in a support around the point where the value of the recovered stress is requested. The method expresses the recovered stress field, for 2D problems, coupling each stress component as shown in (13). For a polynomial of degree N, the basis has $M = (N+2)(N+1)/2$ functions, such that we could write

$$\boldsymbol{\sigma}^*(\mathbf{x}) = \begin{bmatrix} \sigma^*_{xx}(\mathbf{x}) \\ \sigma^*_{yy}(\mathbf{x}) \\ \sigma^*_{xy}(\mathbf{x}) \end{bmatrix} = A(\mathbf{x})\mathbf{p}(\mathbf{x}) = \begin{bmatrix} a_{11}(\mathbf{x}) & \cdots & a_{1M}(\mathbf{x}) \\ a_{21}(\mathbf{x}) & \cdots & a_{2M}(\mathbf{x}) \\ a_{31}(\mathbf{x}) & \cdots & a_{3M}(\mathbf{x}) \end{bmatrix} \begin{bmatrix} p_1(\mathbf{x}) \\ p_2(\mathbf{x}) \\ \vdots \\ p_M(\mathbf{x}) \end{bmatrix} \tag{13}$$

where $\mathbf{p}(\mathbf{x})$ denotes a polynomial basis, and A is the matrix having the coefficients to evaluate, with respect to the basis in $\mathbf{p}$, of each component of the recovered stress $\boldsymbol{\sigma}^*$.

We can use (13) to impose equilibrium constraints in the recovered field $\boldsymbol{\sigma}^*$. Let us consider a point $\mathbf{x}$ with a support $\Omega_\mathbf{x}$, defined by a distance (radius) $R_\mathbf{x}$, and a set of points $\boldsymbol{\chi}$ within $\Omega_\mathbf{x}$, see Figure 2. The size of the support is discussed in [6] for standard FEM formulations. The moving least squares reconstruction for each component of the stress field $\boldsymbol{\sigma}^*(\mathbf{x}) = \boldsymbol{\sigma}^*(\mathbf{x}, \mathbf{x})$ for a point $\boldsymbol{\chi}$ within the support reads

$$\boldsymbol{\sigma}^*(\mathbf{x}, \boldsymbol{\chi}) = A(\mathbf{x})\mathbf{p}(\boldsymbol{\chi}) \quad \forall \boldsymbol{\chi} \in \Omega_\mathbf{x} \tag{14}$$

We use a discrete moving least squares approach, that is motivated by the continuous version [63] via quadrature approximation, to obtain the set A by minimising the functional:

$$\begin{aligned} J(\mathbf{x}) &= \sum_{l=1}^{n} W(\mathbf{x} - \boldsymbol{\chi}_l)[\boldsymbol{\sigma}^*(\mathbf{x}, \boldsymbol{\chi}_l) - \boldsymbol{\sigma}^h(\boldsymbol{\chi}_l)]^2 |\mathbf{J}(\boldsymbol{\chi}_l)| H_l, \\ &\approx \int_{\Omega_\mathbf{x}} W(\mathbf{x} - \boldsymbol{\chi}) \left[\boldsymbol{\sigma}^*(\mathbf{x}, \boldsymbol{\chi}) - \boldsymbol{\sigma}^h(\boldsymbol{\chi})\right]^2 d\boldsymbol{\chi}, \end{aligned} \tag{15}$$

considering the set of n sampling points within the support of $\mathbf{x}$ that will be used as integration points, of coordinates $\boldsymbol{\chi}_l$ ($l = 1...n$). H_l denotes the weight of each point and $|\mathbf{J}(\boldsymbol{\chi}_l)|$ corresponds to the Jacobian determinant. We evaluate at the integration points of the FE analysis, note that each point $\boldsymbol{\chi}_l$ is weighted by $|\mathbf{J}(\boldsymbol{\chi}_l)|H_l$, which represents its associated area.

For the weighting function W, we consider a bell-shaped function commonly used in meshfree methods [63] for the construction of MLS approximations. The function W provides weightings for stress values obtained from the sampling points in the support domain, with farther points having small weights. Also, it ensures that the sampling points leave or enter the support domain gradually, guaranteeing the continuity of the recovered stress field $\boldsymbol{\sigma}^*$. The weighting function is defined as:

$$W(\mathbf{x}-\boldsymbol{\chi}) = \begin{cases} 1-6s^2+8s^3-3s^4 & \text{if } s \leq 1 \\ 0 & \text{if } s > 1 \end{cases} \tag{16}$$

where s is a distance function, normalised within the support $\Omega_{\mathbf{x}}$ and defined as:

$$s = \frac{\|\mathbf{x}-\boldsymbol{\chi}\|}{R_{\mathbf{x}}} \tag{17}$$

The minimisation process results in a system of linear equations $\mathbf{M}(\mathbf{x})A^T(\mathbf{x}) = \mathbf{G}(\mathbf{x})$, where

$$\begin{aligned} \mathbf{M}(\mathbf{x}) &= \sum_{l=1}^{n} W(\mathbf{x}-\boldsymbol{\chi}_l)\,\mathbf{p}(\boldsymbol{\chi}_l)\,\mathbf{p}^T(\boldsymbol{\chi}_l)\,|\mathbf{J}(\boldsymbol{\chi}_l)|H_l \\ \mathbf{G}(\mathbf{x}) &= \sum_{l=1}^{n} W(\mathbf{x}-\boldsymbol{\chi}_l)\,\mathbf{p}(\boldsymbol{\chi}_l)\,(\boldsymbol{\sigma}^h(\boldsymbol{\chi}_l))^T|\mathbf{J}(\boldsymbol{\chi}_l)|H_l. \end{aligned} \tag{18}$$

3.2.1 Satisfaction of the boundary equilibrium equation

From the problem statement, the boundary equilibrium equations should be satisfied along the Neumann boundary. Lagrange Multipliers are used in [8, 64], for an SPR formulation, in order to enforce the equilibrium on patches along the boundary. However, for a MLS recovery, this approach introduces a discontinuity when moving from supports inside the domain to the boundary [6].

We introduce the exact satisfaction of the boundary equilibrium equation smoothly using a *nearest point* approach, thus, avoiding discontinuities in the recovered field. Consider a point $\mathbf{x} \in \Omega$ with a support $\Omega_{\mathbf{x}}$ of radius $R_{\mathbf{x}}$ intersecting the Neumann boundary Γ, as shown in Figure 2. Equilibrium constraints are imposed in the nearest points $\boldsymbol{\chi}_j \in \Gamma$ on the boundaries within the support $\Omega_{\mathbf{x}}$. More than one point can be accounted for depending on the support intersection with the curves that define the boundary.

Let us define a coordinate system $\tilde{x}\tilde{y}$ at $\boldsymbol{\chi}_j$, such that $\tilde{x}$ is the outward normal vector, rotated an angle α with respect to x. The stress vector $\boldsymbol{\sigma}^*(\mathbf{x},\boldsymbol{\chi})$ can be written as:

$$\tilde{\boldsymbol{\sigma}}^*(\mathbf{x},\boldsymbol{\chi}) = \mathbf{R}(\alpha)\boldsymbol{\sigma}^*(\mathbf{x},\boldsymbol{\chi}) \tag{19}$$

being $\mathbf{R}$ a matrix to rotate the stresses:

$$\mathbf{R} = \begin{bmatrix} \mathbf{r}_{\tilde{x}\tilde{x}} \\ \mathbf{r}_{\tilde{y}\tilde{y}} \\ \mathbf{r}_{\tilde{x}\tilde{y}} \end{bmatrix} = \begin{bmatrix} \cos^2\alpha & \sin^2\alpha & \sin(2\alpha) \\ \sin^2\alpha & \cos^2\alpha & -\sin(2\alpha) \\ -\sin(2\alpha)/2 & \sin(2\alpha)/2 & \cos(2\alpha) \end{bmatrix} \tag{20}$$

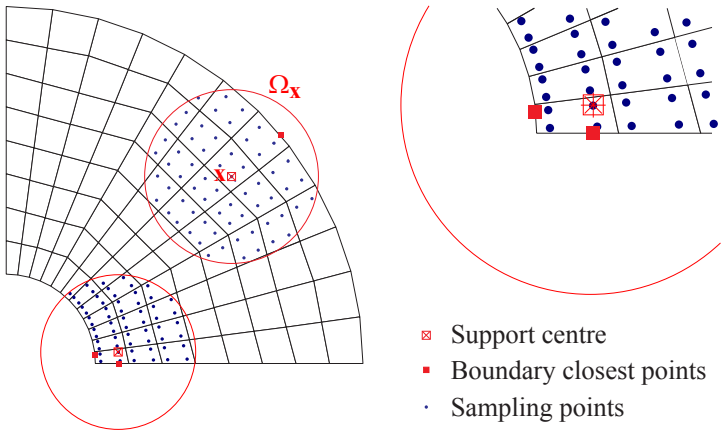

Figure 2: Nearest boundary points to apply boundary conditions in the MLS support.

The continuous MLS functional including the boundary constraints is given by:

$$J(\mathbf{x}) = \sum_{l=1}^{n} W\left(\mathbf{x}-\boldsymbol{\chi}_l\right)\left[\mathbf{A}\left(\mathbf{x}\right)\mathbf{p}(\boldsymbol{\chi}_l) - \boldsymbol{\sigma}^h\left(\boldsymbol{\chi}_l\right)\right]^2 |\mathbf{J}(\boldsymbol{\chi}_l)| H_l + \sum_{j=1}^{nbc} \tilde{W}\left(\mathbf{x}-\boldsymbol{\chi}_j\right)\left[\mathbf{r}_{\tilde{i}}(\alpha)\mathbf{A}\left(\mathbf{x}\right)\mathbf{p}(\boldsymbol{\chi}_j) - \sigma_{\tilde{i}}^{ex}\left(\boldsymbol{\chi}_j\right)\right]^2 \quad \tilde{i} = \tilde{x}\tilde{x}, \tilde{x}\tilde{y} \tag{21}$$

in the above equation, nbc represents the number of points $\boldsymbol{\chi}_j$ were the boundary tractions $\sigma_{\tilde{i}}^{ex}$ are known and constraints are applied. $\tilde{W}$ is a weighting function which reads:

$$\tilde{W}(\mathbf{x}-\boldsymbol{\chi}_j) = \frac{W(\mathbf{x}-\boldsymbol{\chi}_j)}{s} = \begin{cases} \dfrac{1}{s} - 6s + 8s^2 - 3s^3 & \text{if } s \leq 1 \\ 0 & \text{if } s > 1 \end{cases} \tag{22}$$

To guarantee that the weight of the boundary condition in $J(\mathbf{x})$ increases as we approach the Neumann boundary, the function $\tilde{W}$ considers the term s^{-1} (when $\mathbf{x} \to \boldsymbol{\chi}_j$ $s \to 0$) [6]. Further study could include the investigation of other functions to include the boundary conditions. Notice that, as we use integration points inside the elements as sampling points, the recovered stress is not evaluated on the boundary, avoiding singular terms.

3.2.2 Satisfaction of the internal equilibrium equation.

To improve the quality of the recovered stress field we also consider the satisfaction of the internal equilibrium equation in (1) for $\boldsymbol{\sigma}^*$. We impose adequate constraints by means of Lagrange Multipliers.
From (13), the spatial derivatives of $\boldsymbol{\sigma}^*$ are:

$$\nabla \cdot \boldsymbol{\sigma}^* = \mathbf{A}\left(\nabla \cdot \mathbf{p}\right) + \left(\nabla \cdot \mathbf{A}\right)\mathbf{p} \tag{23}$$

The first term in (23) can be directly evaluated differentiating the polynomial basis. The second term in (23) can be obtained by differentiating the linear system $\mathbf{M}\mathbf{A}^T = \mathbf{G}$:

$$(\nabla \cdot \mathbf{M})\,\mathbf{A}^T + \mathbf{M}\left(\nabla \cdot \mathbf{A}^T\right) = \nabla \cdot \mathbf{G} \tag{24}$$

From (24) and (23), we can write:

$$\frac{\partial \boldsymbol{\sigma}^*}{\partial x} = \mathbf{A}\left(\frac{\partial \mathbf{p}}{\partial x} - \mathbf{M}^{-1}\frac{\partial \mathbf{M}}{\partial x}\mathbf{p}\right) + \left(\mathbf{M}^{-1}\frac{\partial \mathbf{G}}{\partial x}\right)^T \mathbf{p} = \mathbf{A}\mathbf{E}_{,x} + \mathbf{f}_{,x} \tag{25}$$

$$\frac{\partial \boldsymbol{\sigma}^*}{\partial y} = \mathbf{A}\left(\frac{\partial \mathbf{p}}{\partial y} - \mathbf{M}^{-1}\frac{\partial \mathbf{M}}{\partial y}\mathbf{p}\right) + \left(\mathbf{M}^{-1}\frac{\partial \mathbf{G}}{\partial y}\right)^T \mathbf{p} = \mathbf{A}\mathbf{E}_{,y} + \mathbf{f}_{,y} \tag{26}$$

Equations (25)-(26) are expressed as a function of $\mathbf{A}$. Thus, the internal equilibrium equations can be rewritten as:

$$\frac{\partial \sigma^*_{xx}}{\partial x} + \frac{\partial \sigma^*_{xy}}{\partial y} + b_x = \left(\mathbf{E}_{xx,x} + \mathbf{E}_{xy,y}\right)\mathbf{A} + \left(f_{xx,x} + f_{xy,y}\right) + b_x = 0 \tag{27}$$

$$\frac{\partial \sigma^*_{xy}}{\partial x} + \frac{\partial \sigma^*_{yy}}{\partial y} + b_y = \left(\mathbf{E}_{xx,y} + \mathbf{E}_{yy,y}\right)\mathbf{A} + \left(f_{xy,x} + f_{yy,y}\right) + b_y = 0. \tag{28}$$

Lagrange Multipliers are used to impose the equilibrium constraints between the coefficients $\mathbf{A}$ from (27)-(28) in (21), leading to:

$$\begin{bmatrix} \mathbf{M} & \mathbf{C}^T \\ \mathbf{C} & \mathbf{0} \end{bmatrix} \begin{bmatrix} \mathbf{A}^T \\ \boldsymbol{\lambda} \end{bmatrix} = \begin{bmatrix} \mathbf{G} \\ \mathbf{Q} \end{bmatrix} \tag{29}$$

where $\boldsymbol{\lambda}$ represents the Lagrange Multipliers and, $\mathbf{C}$ and $\mathbf{Q}$ represent the terms related to the constraint equations. This approach leads to a nearly exact satisfaction of the internal equilibrium equation, as explained in [6].

3.2.3 Visibility

We use the visibility criterion shown in [4, 6] to normalise the distance s in (17) for problems with re-entrant corners and cracks, see Figure 3. For a sampling point $\boldsymbol{\chi}_l$, the weighting function defined by the distance to the point $\mathbf{x}$ is affected by the re-entrant corner at $\boldsymbol{\chi}_\lambda$, such that it decreases as $\boldsymbol{\chi}_l$ cannot be directly viewed from $\mathbf{x}$. The distance function takes the form

$$s = \frac{\|\mathbf{x} - \boldsymbol{\chi}_\lambda\| + \|\boldsymbol{\chi}_l - \boldsymbol{\chi}_\lambda\|}{R_{\mathbf{x}}} \tag{30}$$

3.2.4 Stress splitting for singular problems.

Recovery of stresses works poorly for singular problems as standard procedures cannot capture high gradients of the stress field. A technique which decomposes the stress field into singular and smooth parts was proposed for recovery based error

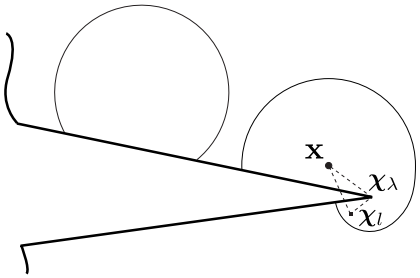

Figure 3: Domain with re-entrant corner.

estimators in [6, 9, 65]. The recovered stress field $\boldsymbol{\sigma}^*$ of the singular problem can be expressed as the linear combination of the singular and non-singular terms:

$$\boldsymbol{\sigma}^* = \boldsymbol{\sigma}^*_{smo} + \boldsymbol{\sigma}^*_{sing} \tag{31}$$

An accurate approximation of the singular part can be evaluated using the asymptotic field expansion near the crack tip given by [10, 66]:

$$\boldsymbol{\sigma}^*_{sing}(r,\phi) = K^*_{\mathrm{I}}\lambda_{\mathrm{I}} r^{\lambda_{\mathrm{I}}-1}\boldsymbol{\Phi}_{\mathrm{I}}(\lambda_{\mathrm{I}},\phi) + K^*_{\mathrm{II}}\lambda_{\mathrm{II}} r^{\lambda_{\mathrm{II}}-1}\boldsymbol{\Phi}_{\mathrm{II}}(\lambda_{\mathrm{II}},\phi) \tag{32}$$

where K^*_{I} and K^*_{II} are estimated values of the generalised stress intensity factors (GSIF) obtained from the FE results using the interaction integral [67]. $\boldsymbol{\Phi}_m$ are trigonometric functions depending on the angular position ϕ, and λ_m ($m = \mathrm{I}, \mathrm{II}$) represent the eigenvalues determining the intensity of the singularity. Notice that the stresses in $\boldsymbol{\sigma}^*_{sing}$ are already equilibrated, as they satisfy the equilibrium equations. A discrete representation of the smooth part $\boldsymbol{\sigma}^h_{smo}$ is obtained by subtracting the singular recovered field:

$$\boldsymbol{\sigma}^h_{smo} = \boldsymbol{\sigma}^h - \boldsymbol{\sigma}^*_{sing} \tag{33}$$

To smooth the discontinuous stress field $\boldsymbol{\sigma}^h_{smo}$ resulting from the splitting, we can use a superconvergent patch recovery technique, as shown in [9, 65]. For polygonal FE elements we propose to use the moving least squares procedure to recover the smooth part of the solution $\boldsymbol{\sigma}^*_{smo}$.

4 Numerical Examples

To investigate the performance of the proposed recovery technique for polygonal elements, we use three 2D benchmark problems with analytical solution. To analyse the results, the global error in energy norm, global effectivity and element effectivity index are used, which we now define.

The global effectivity of the error estimator is calculated as:

$$\theta = \frac{\mathcal{E}}{||\mathbf{e}||} \ . \tag{34}$$

To investigate the local effectivity, we define an element effectivity index, D, as

$$D = \begin{cases} \theta^{\mathrm{e}} - 1\,, & \text{if} \quad \theta^{\mathrm{e}} \geqslant 1 \\ 1 - \dfrac{1}{\theta^{\mathrm{e}}}\,, & \text{if} \quad \theta^{\mathrm{e}} < 1\ , \end{cases} \tag{35}$$

where θ^e is the element effectivity. With this definition, positive values of D indicate elements where the local error is overestimated, and negative values indicate where it is underestimated, with respect to the exact error. In order to calculate θ^e, Equation (12) is used, but with the domain of integration now being the element rather than the physical domain.
For the formulation of the moving least squares support, we consider a second order polynomial basis. Regarding the size of the domain of influence defined by the radius $R_{\mathbf{x}}$, we need a support large enough to have a sufficient number of sampling points for the least squares fitting, but not too large such that we smooth in excess the gradient field. For standard FEM, a good balance between accuracy and local smoothing was obtained for values of $R_{\mathbf{x}}$ equals two times the interpolated value of the average element size at nodes [6]. For polygonal FE approximations, we have chosen a support size with similar conditions, i.e., two times the average element size of surrounding elements.

4.1 A square plate

The first benchmark problem is a model of a 2×2 square plate shown in Figure 4, with material parameters $E = 1000$ for the Young's modulus and $\nu = 0.3$ for the Poisson's ratio. For this problem the exact displacement solution is defined as

$$u(x,y) = x + x^2 - 2xy + x^3 - 3xy^2 + x^2y \tag{36a}$$
$$v(x,y) = -y - 2xy + y^2 - 3x^2y + y^3 - xy^2 \ . \tag{36b}$$

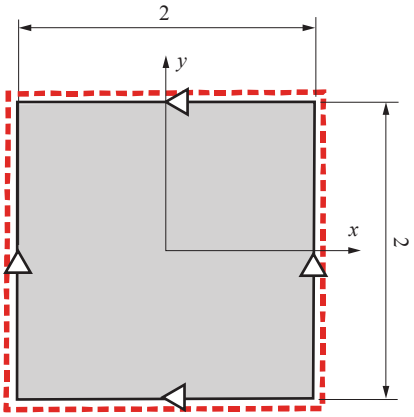

Figure 4: The 2×2 square plate.

Dirichlet boundary conditions are shown as triangles in Figure 4. Displacements in y-direction are constrained at (-1,0) and (1,0), and displacements in x-direction are constrained at (0,-1) and (0,1). Along the Neumann boundary, denoted by a dashed line, we apply the exact values of the stress in (37). The exact stress field obtained

from the displacement field under plane strain conditions reads:

$$\sigma_{xx} = \frac{E}{1+\nu}\left(1 + 2x - 2y + 3x^2 - 3y^2 + 2xy\right) \tag{37a}$$

$$\sigma_{yy} = \frac{E}{1+\nu}\left(-1 - 2x + 2y - 3x^2 + 3y^2 - 2xy\right) \tag{37b}$$

$$\sigma_{xy} = \frac{E}{1+\nu}\left(-x - y + \frac{x^2}{2} - \frac{y^2}{2} - 6xy\right) \ . \tag{37c}$$

Equilibrium condition is guaranteed by applying the body forces

$$b_x(x,y) = -\frac{E}{1+\nu}\,(1+y) \tag{38a}$$

$$b_y(x,y) = -\frac{E}{1+\nu}\,(1-x) \ . \tag{38b}$$

The problem was solved using the polygonal finite element meshes shown in Figure 5. The estimated error in the numerical approximation is evaluated using the moving least squares recovery technique. In Figure 6 the global error norm and the effectivity of the error norm are plotted vs the number of degrees of freedom (DOFs). We compare the results with standard FEM meshes of linear quadrilateral (FEM-Q4) and triangular (FEM-T3) elements using an enhanced moving least squares recovery technique [6]. The rate of convergence of the estimated error in the energy norm for polygonal FEM is approximately 0.5, which is similar to the results obtained for standard FEM and the theoretical convergence rate. The effectivity is within 1% of the ideal value of 1, which means that the estimate of the discretisation error obtained by moving least squares is good for polygonal FEM. The performance of the error estimator is similar to the one observed for linear quadrilateral FEM (FEM-Q4).

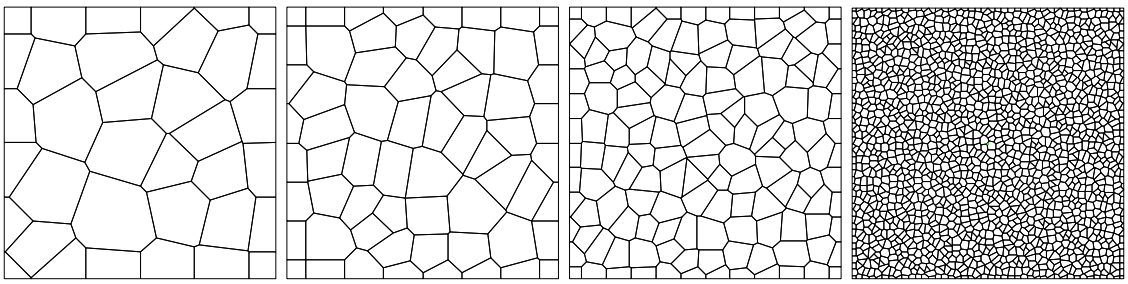

Figure 5: 2×2 square plate. Polygonal finite element meshes

The local effectivity index is plotted for the polygonal meshes in Figure 7. For this smooth problem we notice a balance between underestimated (red colour) and overestimated (blue colour) errors in the elements. Dark blue and dark red indicate top of the scale. The local effectivity index D is within a range of $[-0.4, 0.4]$, which is in agreement with the results reported in the literature for standard FEM [6].

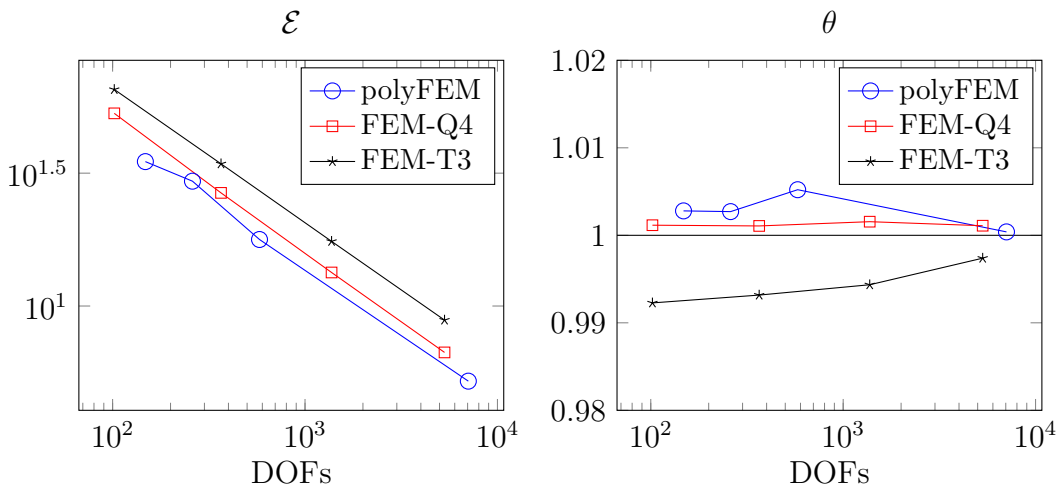

Figure 6: 2×2 square plate. Global estimated error in energy norm and effectivity, θ, for polygonal (polyFEM), linear quadrilateral (FEM-Q4) and triangular (FEM-T3) elements.

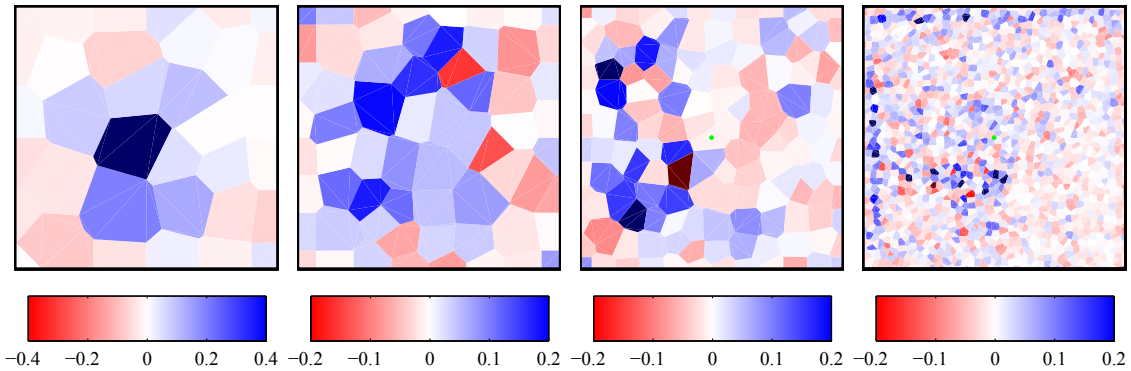

Figure 7: 2×2 square plate. Local effectivity index D for polygonal FEM

4.2 Thick-walled cylinder subject to an internal pressure

The geometrical model for the thick-walled cylinder considering symmetry conditions is shown in Figure 8. The exact solution for this problem is given for a point (x, y) in cylindrical coordinates. Denoting $c = b/a$ and $r = \sqrt{x^2 + y^2}$, the radial displacement can be written as

$$u_r = \frac{P(1+\nu)}{E(c^2-1)}\left(r\,(1-2\nu) + \frac{b^2}{r}\right) \tag{39}$$

Stresses can be derived from the known displacements, and read

$$\sigma_r = \frac{P}{c^2-1}\left(1-\frac{b^2}{r^2}\right), \quad \sigma_t = \frac{P}{c^2-1}\left(1+\frac{b^2}{r^2}\right), \quad \sigma_z = 2\nu\frac{P}{c^2-1}. \tag{40}$$

In Figure 9 we show the set of polygonal meshes used to solve the cylinder problem. The global error norm and its effectivity are shown in Figure 10. The convergence rate for polyFEM is 0.6, for FEMQ4 is 0.51 and for FEMT3 is 0.49, which are close

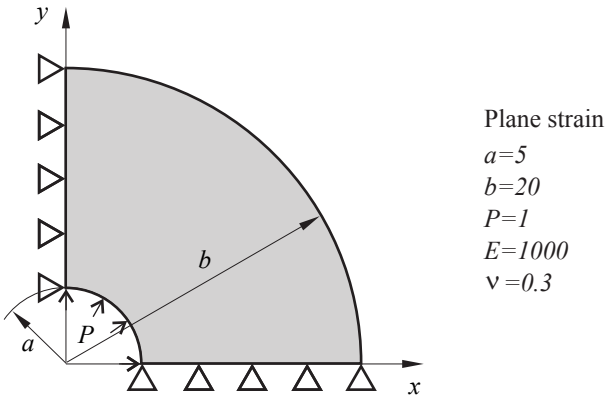

Figure 8: Thick-walled cylinder subject to internal pressure.

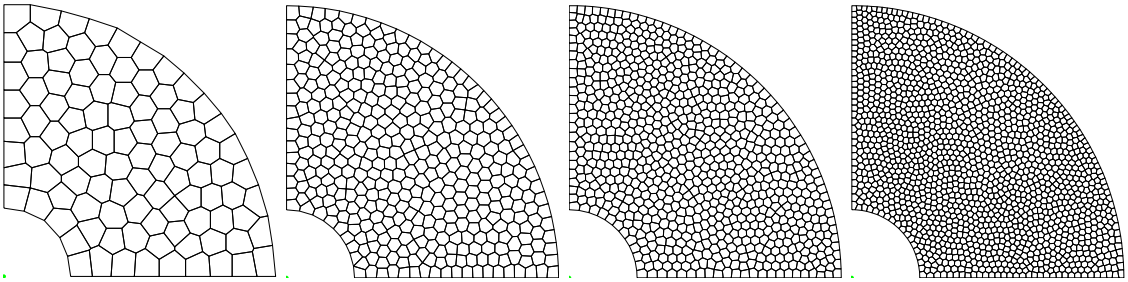

Figure 9: Thick-walled cylinder. Polygonal finite element meshes.

to the theoretical convergence rate. The global effectivity is very close to the ideal value of 1, indicating that the estimation of the error is good for the polygonal meshes used in this study.

Note that the stress field recovered by the proposed technique is not statically admissible, therefore, although the error estimation is quite close to the exact error ($\theta \approx 1$), the error estimate is not necessarily an overestimation of the exact error. For this problem, the accuracy of the estimated error for polyFEM meshes is similar to the accuracy obtained for FEM, although the polyFEM results underestimate the exact error whereas the FEM results, except for one of the FEMT3 meshes, overestimate it. In any case, the results always provide effectivities within the range [0.8,1.2]. According to the literature [66], it could be desired that the effectivity index be such that $0.8 \leq \theta \leq 1.2$ and $\theta \to 1$.

Figure 11 shows the element effectivity index for each of the four meshes. For the coarse mesh, the element error is less well approximated on the outer boundary of the cylinder. On increasing mesh density, the quality of the approximation of the error becomes more uniform throughout the domain. The same behaviour was observed for FEM approximations [6].

4.3 L-shaped domain under mode I loading

The singular elasticity problem of a finite portion of an infinite domain with a reentrant corner is shown in Figure 12.

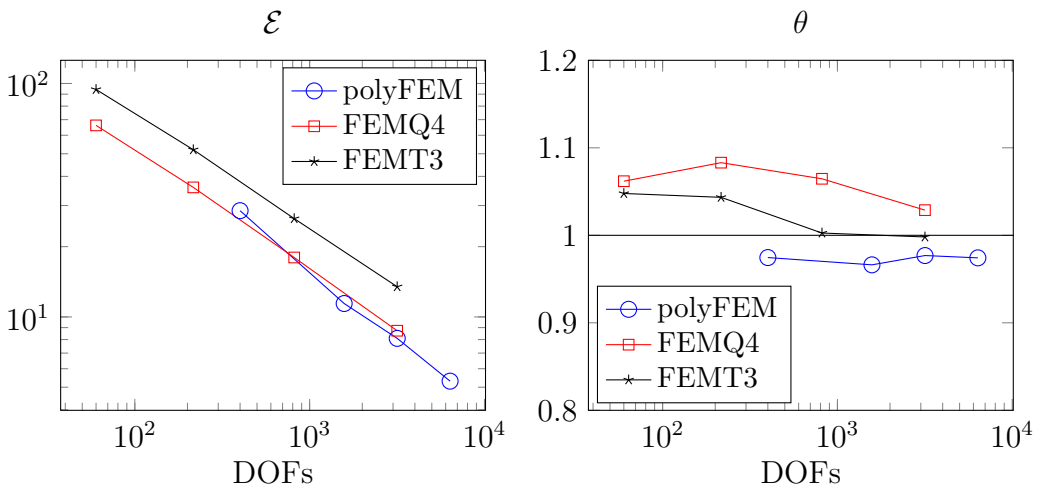

Figure 10: Thick-walled cylinder. Global estimated error in energy norm and effectivity, θ, for polygonal (polyFEM), linear quadrilateral (FEM-Q4) and triangular (FEM-T3) elements.

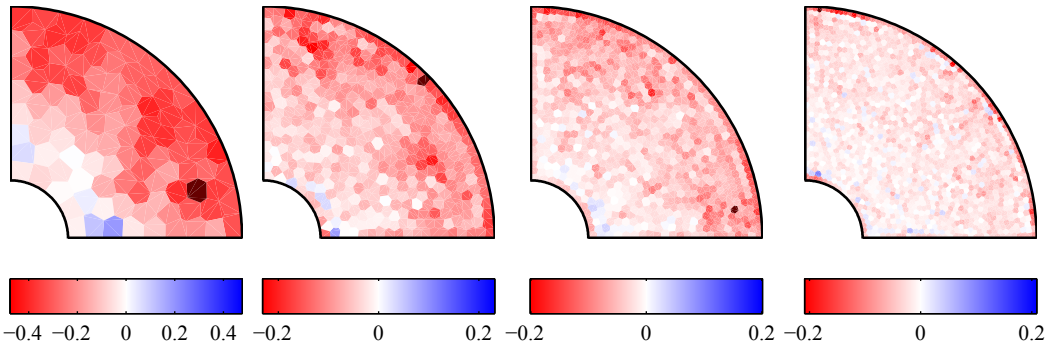

Figure 11: Thick-walled cylinder. Local effectivity index D for polygonal FEM.

Neumann boundary conditions are indicated by thick, dashed lines. The applied tractions are evaluated from the first terms of the asymptotic expansion describing the exact solution under mixed mode loading conditions.

The exact solution for the displacements and stresses for this problem can be found in [10,66]. The problem exhibits a singular solution in the vertex. To model mode I loading conditions, we fix the exact values of the generalised stress intensity factors (GSIF) to $K_{\mathrm{I}} = 1$ and $K_{\mathrm{II}} = 0$ [66]. Material parameters are Young's modulus $E = 1000$ and Poisson's ratio $\nu = 0.3$. For this singular problem, we apply the *singular+smooth* stress splitting procedure as explained in Section 3.2.4. We use an equivalent domain integral to obtain an approximation of the stress intensity factors that describes the recovered singular part.

The final benchmark test will demonstrate the improved performance of MLSCX when compared with a standard MLS, which is not especially designed for problems with singularities. First, the problem is solved on four meshes using a MLS recovery which does not consider equilibrium conditions and singular stress splitting. Then, the problem is solved again on the same four meshes, but, the stress solution is

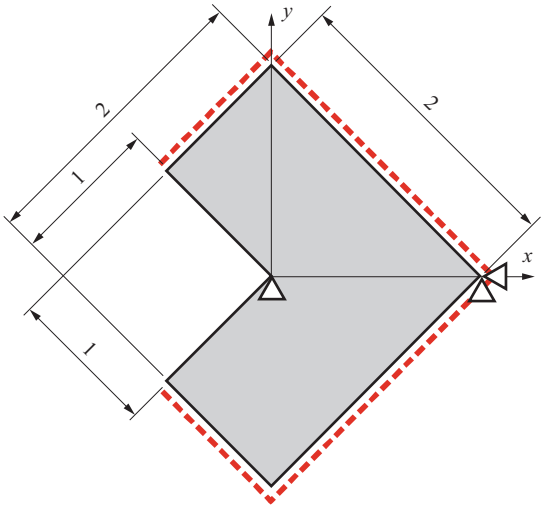

Figure 12: L-shaped domain under mode I load.

decomposed into smooth and singular parts, and the recovered stress field is forced to satisfy equilibrium, referred to as MLSCX. In Figure 13 we show the set of polygonal meshes used to solve the L-shaped problem problem.

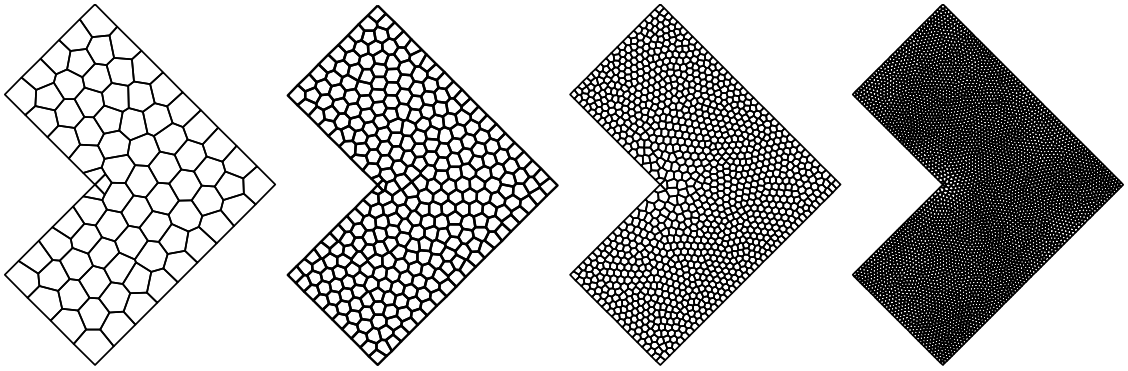

Figure 13: L-shaped domain. Polygonal finite element meshes.

The global effectivities are plotted for both sets of results in Figure 14. We can observe that for basic MLS recovery, the effectivity is above the desire value of 1.2. For the enhanched MLSCX, the global effectivity is closer to 1, as observed in previous examples. The convergence rate of the error in energy norm for the two recovery approaches is near 0.23, which is in agreement with the theoretical convergence rate for this singular problem under uniform refinement conditions, i.e. 0.272.

The local effectivity index, D, is shown for each mesh in Figures 15 (MLS) and 16 (MLSCX). For the error estimate based on MLS, the value of the effectivity index is overestimated near the singular corner. For the enhanced error estimator, the effectivity index is much improved at the corner, where it is closer to the ideal value of 0. Therefore, at the corner, the enhanced recovery technique gives a more accurate approximation of the error. This improvement is mostly due to the splitting

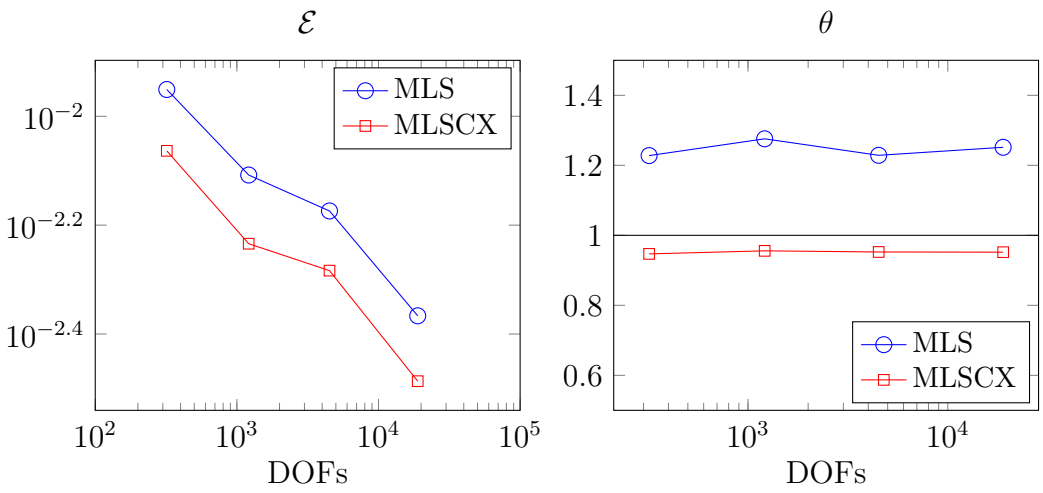

Figure 14: L-shaped domain. Global estimated error in energy norm and effectivity, θ, for MLS and MLSCX stress recovery.

of the stress field and this behaviour is similar for standard FE approximations. Underestimated areas on the right are due to pollution error effects, as observed in FE meshes with uniform refinement.

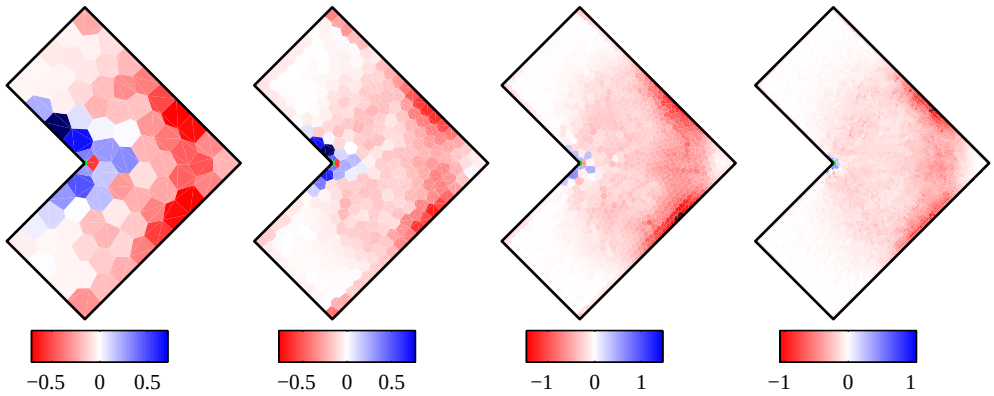

Figure 15: L-shaped domain. Local effectivity index D for the error estimator based on MLS recovery.

5 Conclusions

In this paper, we have presented a novel technique to estimate the discretization error in arbitrary polygonal finite element meshes for smooth and singular elasticity problems. The MLSCX technique is based on an enhanced moving least squares recovery which considers internal and boundary equilibrium conditions to improve the quality of the recovered stress field. For singular problems, the MLSCX also involves a stress splitting procedure to separately recover the smooth and singular parts of the stress field.

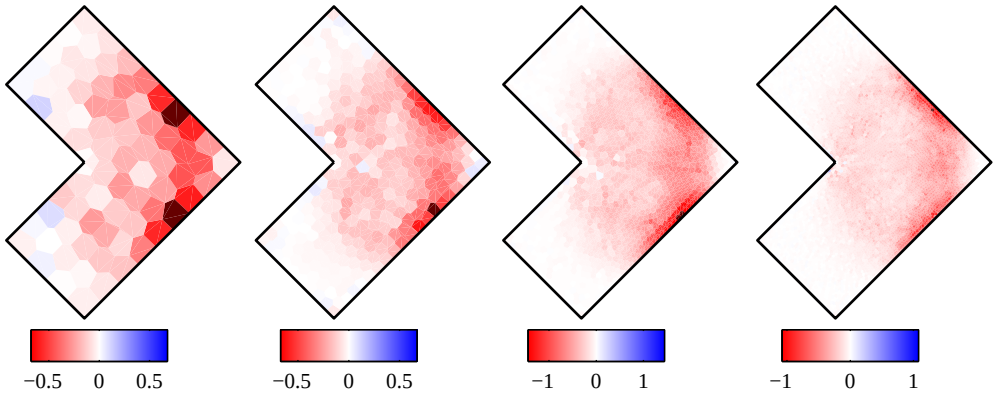

Figure 16: L-shaped domain. Local effectivity index D for the error estimator based on enhanced MLSCX recovery.

We have used three benchmark problems with known solution to assess the performance of the MLSCX recovery: two problems with an smooth solution and one singular problem. For smooth problems, results show the good performance of the error measure obtained with the proposed method, both globally and locally at element level. The obtained convergence rate for the estimated error was 0.5, similar to the rate observed for standard finite element approximations. The global effectivity θ was within the recommended range $[0.8, 1.2]$. We have tested the singular problem of a plate with a reentrant corner under mode I loading conditions. Numerical results show that the stress splitting improves the error measure in the vicinity of the crack tip and the values of θ are also close to one. Convergence rate of the estimated error is lower than for smooth problems (0.23), due to the intensity of the singularity. Similar performance was observed for conventional FE singular models. Results indicate that the proposed error estimator technique for arbitrary polygonal FE meshes yields good error measures, and could be used to control the error in this kind of numerical approximations.

6 Acknowledgements

This work was partially funded by the EPSRC grant EP/G042705/1 "Increased Reliability for Industrially Relevant Automatic Crack Growth Simulation with the eXtended Finite Element Method", the Framework Programme 7 Initial Training Network Funding under grant number 289361 "Integrating Numerical Simulation and Geometric Design Technology", and Convocatoria Interna VIE 2522, Universidad Industrial de Santander. Stéphane Bordas also thanks partial funding for his time provided by the European Research Council Starting Independent Research Grant (ERC Stg grant agreement No. 279578) "RealCut Towards real time multiscale simulation of cutting in non-linear materials with applications to surgical simulation and computer guided surgery".

References

[1] Ainsworth M, Oden JT. *A posteriori Error Estimation in Finite Element Analysis*. John Wiley & Sons: Chichester, 2000.

[2] Zienkiewicz OC, Zhu JZ. A simple error estimator and adaptive procedure for practical engineering analysis. *International Journal for Numerical Methods in Engineering* 1987; **24**(2):337–357.

[3] Zienkiewicz OC, Zhu JZ. The superconvergent patch recovery and a posteriori error estimates. Part 1: The recovery technique. *International Journal for Numerical Methods in Engineering* ; (7):1331–1364.

[4] Bordas SPA, Duflot M. Derivative recovery and a posteriori error estimate for extended finite elements. *Computer Methods in Applied Mechanics and Engineering* 2007; **196**(35-36):3381–3399.

[5] Xiao QZ, Karihaloo BL. Statically admissible stress recovery using the moving least squares technique. *Progress in Computational Structures Technology*, Topping BHV, Soares CAM (eds.), Saxe-Coburg Publications: Stirling, Scotland, 2004; 111–138.

[6] Ródenas JJ, González-Estrada OA, Fuenmayor FJ, Chinesta F. Enhanced error estimator based on a nearly equilibrated moving least squares recovery technique for FEM and XFEM. *Computational Mechanics* aug 2013; **52**(2):321–344, doi:10.1007/s00466-012-0814-7.

[7] Zienkiewicz OC, Taylor R. *The Finite Element Method: The Basis*, vol. 1. 5 edn., Butterworth-Heinemann: Oxford, UK, 2000.

[8] Ródenas JJ, Tur M, Fuenmayor FJ, Vercher A. Improvement of the superconvergent patch recovery technique by the use of constraint equations: the SPR-C technique. *International Journal for Numerical Methods in Engineering* 2007; **70**(6):705–727, doi:10.1002/nme.1903.

[9] Ródenas JJ, González-Estrada OA, Tarancón JE, Fuenmayor FJ. A recovery-type error estimator for the extended finite element method based on singular+smooth stress field splitting. *International Journal for Numerical Methods in Engineering* 2008; **76**(4):545–571, doi:10.1002/nme.2313.

[10] González-Estrada O, Natarajan S, Ródenas J, Nguyen-Xuan H, Bordas S. Efficient recovery-based error estimation for the smoothed finite element method for smooth and singular linear elasticity. *Computational Mechanics* 2012; :1–16.

[11] Moorthy S, Ghosh S. Adaptivity and convergence in the Voronoï cell finite element method for analyzing heterogeneous materials. *Computer Methods in Applied Mechanics and Engineering* 2000; **185**:37–74.

[12] Dasgupta G. Interpolants within Convex Polygons: Wachspress' Shape Functions. *ASCE - Journal of aerospace engineering* 2003; **16**(1):1–8.

[13] Sze K, Sheng N. Polygonal finite element method for nonlinear constitutive modeling of polycrystalline ferroelectrics. *Finite Elements in Analysis and Design* 2005; **42**(2):107–129.

[14] Pavankumar P, Jayabal K, Arockiarajan A. A comparative study between finite element and polygonal finite element approaches for electromechanical coupled linear problems. *Intergrated Ferroelectrics* 2010; **120**:90–101.

[15] Jayabal K, Menzel A, Arockiarajan A, Srinivasan S. Micromechanical modelling of switching phenomena in polycrystalline piezoceramics: application of a polygonal finite element approach. *Computational Mechanics* 2011; **48**:421–435.

[16] Kraus M, Rajagopal A, Steinmann P. Investigations on the polygonal finite element method constrained adaptive delaunay tessellation and conformal interpolants. *Computers & Structures* 2013; **120**:33–46.

[17] Floater MS. Mean value coordinates. *Computer Aided Geometric Design* 2003; **20**(1):19–27.

[18] Warren J, Schaefer S, Hirani A, Desbrun M. Barycentric coordinates for convex sets. *Advances in Computational Mechanics* 2007; **27**(3):319–338.

[19] Wachspress EL. A rational basis for function approximation. *Lecture notes in Mathematics* 1971; .

[20] Sukumar N, Malsch E. Recent Advances in the Construction of Polygonal Finite Element Interpolants. *Archives of Computational Methods in Engineering* 2006; **13**(1):129–163.

[21] Arroyo M, Ortiz M. Local Maximum-Entropy Approximation Schemes. *Lecture notes in Computational Science and Engineering* 2006; **57**:1.

[22] Rashid M, Gullet P. On a finite element method with variable element topology. *Computer Methods in Applied Mechanics and Engineering* 2000; **190**(11–12):1509–1527.

[23] Ghosh S, Liu Y. Voronoï cell finite element model-based on micropolar theory of thermoelasticity for heterogeno us materials. *Internation Journal of Numerical Methods in Engineering* 1995; **38**:1361–1398.

[24] Ghosh S, Moorthy S. Elastic-plastic analysis of arbitrary heterogeneous materials with the Voronoï-cell finite element method. *Comput. Meth. Appl. Mech. Eng.* 1995; **121**:373–[409.

[25] Tiwary A, Hu C, Ghosh S. Numerical conformal mapping method based Voronoï cell finite element model for analyzing microstructures with irregular heterogeneities. *Finite Element in Analysis and Design* 2007; **43**:504–520.

[26] Tang X, Wu S, Zheng C, Zhang J. A novel virtual node method for polygonal elements. *Appl. Math. Mech.* 2009; **30**(10):1233–1246.

[27] Beirão da Veiga L, Brezzi F, Cangiani A, Manzini G, Marini LD, Russo A. Basic principles of virtual element methods. *Mathematical Models and Methods in Applied Sciences* 2013; **23**:199.

[28] Ooi ET, Song C, Tin-Loi F, Yang Z. Polygon scaled boundary finite elements for crack propagation modelling. *International Journal for Numerical Methods in Engineering* 2012; **91**:319–342.

[29] Natarajan S, Ooi ET, Chiong I, Song C. Convergence and accuracy of displacement based finite element formulation over arbitrary polygons: Laplace interpolants, strain smoothing and scaled boundary polygon formulation. *Finite Elements in Analysis and Design* 2014; **85**:101–122.

[30] Francis A, Ortiz-Bernardin A, Bordas SP, Natarajan S. Linear smoothed polygonal and polyhedral finite elements. *International Journal for Numerical Methods in Enginering* 2016; .

[31] Rjasanow S, Weißer S. Higher order BEM-based FEM on polygonal meshes. *SIAM J Numer Anal* 2012; **50**:2357–2378.

[32] Barros FB, de Barcellos CS, Duarte CA. p-Adaptive C^k generalized finite elemnet method for arbitrary polygonal clouds. *Computational Mechanics* 2007; **41**:175–187.

[33] Cangiani A, Manzini G, Russo A, Sukumar N. Hourglass stabilization and the virtual element method. *International Journal for Numerical Methods in Engineering* 2015; **102**:404–436.

[34] Natarajan S, Bordas S, Ooi ET. Virtual and smoothed finite elements: a connection and its application to polygonal/polyhedral finite element methods. *International Journal for Numerical Methods in Engineering* 2015; .

[35] Weißer S. Residual error estimate for BEM-based FEM on polygonal meshes. *Numerische Mathematik* 2011; **118**(4):765–788, doi:10.1007/s00211-011-0371-6.

[36] Hofreither C. L 2 error estimates for a nonstandard finite element method on polyhedral meshes 2011; **19**(1):27–39.

[37] Di Pietro DA, Ern A, Lemaire S. An arbitrary-order and compact-stencil discretization of diffusion on general meshes based on local reconstruction operators. *Computational Methods in Applied Mathematics* 2014; **14**(4):461–472, doi:10.1515/cmam-2014-0018.

[38] Beirão da Veiga L, Manzini G. Residual *a posteriori* error estimation for the Virtual Element Method for elliptic problems. *ESAIM: Mathematical Modelling and Numerical Analysis* 2015; **49**(2):577–599, doi:10.1051/m2an/2014047.

[39] González-Estrada OA, Natarajan S, Ródenas JJ, Bordas SPA, Heaney C. Recovery-Based Error Estimation for the Polygonal Finite Element Method

for Smooth and Singular Linear Elasticity. *11th World Congress on Computational Mechanics*, Oñate E, Oliver X, Huerta A (eds.), WCCM XI, CINME: Barcelona, 2014; 1–2.

[40] Kasi B, Rajagopal A, Steinmann P. Adaptive Poly-FEM for the analysis of plane elasticity problems. *International Journal for Computational Methods in Engineering Science and Mechanics* 2017; **18**(2-3):146–165.

[41] Chi H, Beirão da Veiga L, Paulino GH. A simple and effective gradient recovery scheme and a posteriori error estimator for the Virtual Element Method (VEM). *Computer Methods in Applied Mechanics and Engineering* apr; :21–58doi:10.1016/j.cma.2018.08.014.

[42] Sukumar N, Tabarraei A. Conforming polygonal finite elements. *International Journal of Numerical Methods in Engineering* 2004; **61**:2045–2066.

[43] Floater MS. Wachspress and mean value coordinates. *Approximation Theory XIV: San Antonio 2013*, Fasshauer GE, Schumaker LL (eds.), Springer International Publishing: Cham, 2014; 81–102.

[44] Wachspress E. *Rational Bases and Generalized Barycentrics, Applications to Finite Elements and Graphics*. Springer: Cham, doi:10.1007/978-3-319-21614-0.

[45] Sibson R. A vector identity for Dirichlet tessellaton. *Mathematical Proceedings of the Cambridge Philosophical Society* 1980; **87**:151–155.

[46] Cueto E, Sukumar N, Calvo B, Martinez M, Cegoñino J, Doblaré M. Overview and recent advances in natural neighbour Galerkin methods. *Archives of Computational Methods in Engineering* 2003; **10**(4):307–384.

[47] Yoo JW, Moran B, Chen JS. Stabilized conforming nodal integration in the natural-element method. *International Journal for Numerical Methods in Engineering* 2004; **60**(5):861–890, doi:10.1002/nme.972.

[48] Sukumar N, Moran B, Belytschko T. The natural element method in solid mechanics. *International Journal of Numerical Methods in Engineering* 1998; **43(5)**:839–887.

[49] Sukumar N. The Natural Element Method in Solid Mechanics. PhD Thesis, Theoretical and Applied Mechanics, Northwestern University, Evanston, IL, U.S.A 1998.

[50] Chris N, Friedberg R, Lee T. Weights of links and plaquettes in a random lattice. *Nuclear Physics* 1982; **210**:337–346.

[51] Belikov V, Ivanov V, Kontorovich V, Korytnik S, Semenow AY. The non-Sibsonian interpolation: A new method of interpolation of the values of a function on an arbitrary set of points. *Computational Mathematics and Mathematical Physics* 1997; **37**:9–15.

[52] Hiyoshi H, Sugihara K. Two generalizations of an interpolant based on Voronoï diagrams. *Int. J. Shape Modeling* 1999; **5**(2):219–231.

[53] Hormann K, Sukumar N ((eds.)). *Generalized Barycentric Coordinates in Computer Graphics and Computational Mechanics*. CRC Press: Boca Raton, 2017, doi:10.1201/9781315153452.

[54] Natarajan S, Bordas SPA, Mahapatra DR. Numerical integration over arbitrary polygonal domains based on Schwarz-Christoffel conformal mapping. *International Journal for Numerical Methods in Engineering* 2009; **80**(1):103–134, doi: 10.1002/nme.

[55] Mousavi S, Xiao H, Sukumar N. Generalized Gaussian quadrature rules on arbitrary polygons. *International Journal for Numerical Methods in Engineering* 2010; **82**(1):99–113.

[56] Nguyen-Thoi T, Liu G, Nguyen-Xuan H. An $n-$sided polygonal edge-based smoothed finite element method nES-FEM for solid mechanics. *International Journal for Numerical Methods in Engineering* 2011; **27**:1446–1472.

[57] Lyness J, Monegato G. Quadrature rules for regions having regular hexagon symmetry. *SIAM Journal on Numerical Analysis* 1977; **14**(2):283–295.

[58] Sommariva A, Vianello M. Gauss-green cubature and moment computation over arbitrary geometries. *Journal of Computational and Applied Mathematics* 2009; **231**(2):886–896.

[59] Thiagarajan V, Shapiro V. Adaptively weighted numerical integration over arbitrary domains. *Technical Report*, University of Wisconsin-Madison 2013.

[60] Chin EB, Lasserre JB, Sukumar N. Numerical integration of homogeneous functions on convex and non-convex polygons and polyhedra. *Computational Mechanics* 2015; **56**:967–981.

[61] Wiberg NE, Abdulwahab F, Ziukas S. Enhanced superconvergent patch recovery incorporating equilibrium and boundary conditions. *International Journal for Numerical Methods in Engineering* Oct 1994; **37**(20):3417–3440, doi: 10.1002/nme.1620372003.

[62] Maunder EAW. A Trefftz patch recovery method for smooth stress resultants and applications to Reissner-Mindlin equilibrium plate models. *Computer Assisted Mechanics and Engineering Sciences* 2001; **8**(2-3):409–424.

[63] Liu GR. MFree Shape Function Construction. *Mesh Free Methods. Moving beyond the Finite Element Method*. chap. 5, CRC Press: Boca Ratón, Florida, 2003; 693.

[64] Ródenas JJ, González-Estrada OA, Díez P, Fuenmayor FJ. Accurate recovery-based upper error bounds for the extended finite element framework. *Computer Methods in Applied Mechanics and Engineering* 2010; **199**(37-40):2607–2621.

[65] Ródenas JJ, Giner E, Tarancón JE, González-Estrada OA. A recovery error estimator for singular problems using singular+smooth field splitting. *Fifth International Conference on Engineering Computational Technology*, Topping BHV, Montero G, Montenegro R (eds.), Civil-Comp Press: Stirling, Scotland, 2006.

[66] Szabó BA, Babuška I. *Finite Element Analysis*. John Wiley & Sons: New York, 1991.

[67] Giner E, Tur M, Fuenmayor FJ. A domain integral for the calculation of generalized stress intensity factors in sliding complete contacts. *International Journal of Solids and Structures* Feb 2009; **46**(3-4):938–951, doi:10.1016/j.ijsolstr.2008.10.007.